Three-dimensional domain growth on the size scale of the capillary length: Effective growth exponent and comparative atomistic and mean-field simulations

Matthias Strobel,[1,2,*] Karl-Heinz Heinig,[1] and Wolfhard Möller[1,3]
[1]*Forschungszentrum Rossendorf, Institut für Ionenstrahlphysik und Materialforschung, Postfach 510 119, D-01314 Dresden, Germany*
[2]*MIRIAM, Universitá degli studi di Milano, Via C. Saldini 50, I-20133 Milano, Italy*
[3]*Technische Universität Dresden, Institut für Oberflächen- und Mikrostrukturphysik, Zellescher Weg 16, D-01069 Dresden, Germany*
(Received 22 June 2001; published 10 December 2001)

The evolution of diffusively interacting nanoclusters is investigated by combined atomistic (kinetic lattice Monte Carlo method based on the nearest-neighbor Ising model) and mean-field (numerical integration of the governing reaction-diffusion equations) simulations. By expressing Monte Carlo parameters in terms of macroscopic thermodynamic quantities a well-defined interface between both methods is derived. Based on extensive Monte Carlo studies of the Gibbs-Thomson equation an explicit expression for the intrinsic capillary length is presented. Starting with high-temperature quenches, the evolution of nanoclusters is first studied by the atomistic model. The observed transient dynamics of coarsening is explained uniquely on the basis of the ratio of the capillary length to the mean cluster size. Using input data from the atomistic model, Ostwald ripening is also studied in parallel with the mean-field model. In a detailed study, the similarities and differences of both approaches are discussed and explained in terms of their statistical and deterministic natures. It is demonstrated that in contrast to the commonly applied linearized version of the Gibbs-Thomson relation in the mean-field approach only the use of the full exponential form provides a reasonable matching with the atomistic model.

DOI: 10.1103/PhysRevB.64.245422 PACS number(s): 68.35.Md, 05.50.+q, 64.60.My, 64.75.+g

I. INTRODUCTION

Recently, nanoclusters have attracted much interest due to their unique physical properties as essentially zero-dimensional objects. This is additionally motivated by their use in new technological devices, which exploit size effects on a nanometer scale. For instance, nonlinear optical properties of metallic nanoclusters in insulators are based on the size dependence of the plasmon frequency.[1] A further example is the use of (semiconducting) nanoclusters in the thin-gate oxide of conventional transistor structures for novel nonvolatile memory devices.[2]

A variety of techniques have been developed to produce nanoclusters in different ambients, e.g., by ion beam synthesis in near-surface layers of solids.[3–5] In most of these methods average properties of (finite) nanocluster ensembles like their mean size $\langle R\rangle$ and their number density n can be controlled to a large extent. This knowledge of the general features of nanocluster evolution has been obtained from extensive studies of various aspects of phase transformation phenomena in homogeneous systems. A rather good understanding of the concepts of nanocluster formation due to the decay of a metastable system has been developed from theoretical studies of (homogeneous) nucleation and growth mechanisms of second-phase domains.[6–8] This has been supported by extensive computer simulations, especially with Monte Carlo (MC) methods.[9] These atomistic approaches have been used to test the predictions of classical nucleation theory as well as to study in detail the kinetics of the early stages of first-order phase transitions.[10–12]

The late stage of the evolution of isolated, diffusionally interacting clusters is commonly described in the framework of Ostwald ripening (OR). This process is driven by the minimization of the surface energy associated with the precipitate-matrix interface, which causes large clusters to grow at the expense of small ones. A comprehensive theory of OR in three-dimensional (3D) space was first developed by Lifshitz and Slyozov[13] and independently by Wagner[14] (LSW theory) in the limit of vanishing volume fraction $\phi \rightarrow 0$ of the minority phase. LSW derived the time dependence of OR in the asymptotic limit, which, for $t\rightarrow\infty$, reads $\langle R\rangle \propto t^m$ with $m=1/3$ in the case of diffusion control (a similar relation with growth exponent $m=1/2$ holds in the in case of interface reaction control[14]). Additionally, they predicted a stationary form of the particle radius distribution (PRD) in terms of the scaled cluster size $\rho = R/\langle R\rangle$. As a consequence of the LSW theory in the late stage of phase separation all physical quantities should depend only on a single length scale l, e.g., on the average domain size $\langle R\rangle$ (scaling hypothesis; see, e.g., the reviews of Furukawa[15] and Bray[16]). Essentially all later work on coarsening refers to the LSW theory.

Based on a global mean-field description, the LSW theory does not take into account explicitly the effects of diffusional interactions among nanoclusters and the resulting modifications of the governing kinetic equation of cluster growth. A variety of modifications of the original LSW theory have been proposed in order to tackle the peculiarities of OR at finite volume fractions $\phi > 0$.[17–22] Although the derived growth rates differ, all models agree that the growth exponent m does not change in the asymptotic limit. Recently, in an advanced coarsening experiment the predictions for (transient) OR, i.e., the coarsening rate and the growth exponent, have been verified.[23]

The starting point for most numerical investigations of OR is the multiparticle diffusion equation which has to fulfill appropriate boundary conditions at the precipitate-matrix in-

terfaces. Deriving a solution based on the monopole approximation of nanocluster interactions, which corresponds to assuming pointlike sources and sinks for the dissolved phase, the OR characteristics of ensembles of several thousand precipitates has been studied.[22,24–27] Despite particular differences in the numerical approaches in all these local mean-field simulations the LSW-growth exponent for diffusion-controlled ripening has been verified. For appropriate modifications of the precipitate-matrix boundary conditions also the LSW predictions for reaction-controlled OR have been checked.[28–30]

While MC simulations are the method of choice to study the kinetics of first-order phase transitions, there has been a long-standing discussion about the dynamics of these models, especially with respect to the predictions of the LSW theory. This is based on the fact that MC methods are computationally orders of magnitude more expensive than mean-fields models; thus, especially in three dimensions, simulated systems hardly ever reach the coarsening stage, where the application of the LSW theory is justified.

Using the kinetic Ising model [usually restricted to nearest-neighbor (NN) interactions] MC studies in two (mostly on a square lattice) (Refs. 31–34) and three (mostly on a simple cubic lattice) (Refs. 35–37 and 10) dimensions of the growth of minority phase domains in systems with conserved and nonconserved order parameters have been performed for many years (see, e.g., Gunton *et al.*[9] for a comprehensive review of the work up to 1983). Motivated by available experimental techniques, MC studies on three-dimensional domain growth first focused on the properties of the structure function (the Fourier transform of the two-particle correlation function), because phase separating systems have been mainly investigated by scattering experiments. With the upcoming advent of direct detection systems for nanoclusters, in particular high-resolution transmission electron microscopy, characterizations of ensembles of nanoclusters in terms of individual and mean sizes as well as size distributions have become more and more popular.

Using a simple cubic lattice gas model, Penrose *et al.*[38] simulated cluster growth after a quench ($T=0.59T_c$, where T_c denotes the critical intrinsic temperature, above which no phase transition exists) below the coexistence curve into the metastable region. For a system with a volume fraction $\phi=0.075$ they reported a linear dependence of the critical nanocluster size $i^\star$ on time for a run of 6000 MC steps. Further MC studies in three dimensions with explicit analysis according to the droplet model have been performed, for instance, by Lebowitz *et al.*,[10] Kalos *et al.*,[11] and Penrose *et al.*,[12] who concentrated on a detailed kinetic description of the phase transition. Surprisingly, since the middle 1980s further work on domain coarsening in three dimensions using the kinetic Ising model has been very hard to find.[39,40] It is also noteworthy that essentially all published studies have concentrated on rather high intrinsic temperatures, i.e., $T_c/10 \lesssim T \approx T_c$. However, as will be shown below, for K3DLMC descriptions of a variety of physically and technologically interesting phase-separation systems, appropriate intrinsic temperatures are in the range $T<T_c/10$.

The purpose of this work is twofold. First we would like to revisit the kinetic lattice MC approach to three-dimensional domain growth with respect to the dynamics and the effective growth exponent m. We reformulate the problem by characterizing late-stage coarsening conditions in terms of the ratio $R_c/\langle R\rangle$, where R_c denotes the capillary length. More precisely we present evidence that the effective growth exponent is a unique function of the ratio $R_c/\langle R\rangle$ only. Then, based on a well-defined interface between atomistic and mean-field simulation models, by simulating in parallel the evolution of a particular ensemble of nanoclusters we present the similarities and differences of both approaches with respect to OR. It is demonstrated that in contrast to the commonly applied linearized version of the Gibbs-Thomson relation in the mean-field approach only the use of the full exponential form provides a reasonable matching with the atomistic model.

The remainder of this paper is organized as follows. Section II starts with a description of the atomistic model which is followed by the gauging of the MC parameters and ends by an exploration of the Gibbs-Thomson equation and the derivation of an expression for the surface tension. The standard mean-field model of OR is introduced in Sec. III. The results of MC simulations of three-dimensional domain growth and its dynamic interpretation are presented in Sec. IV. This is followed by a detailed comparative study of the evolution of a particular system by both methods.

II. KINETIC THREE-DIMENSIONAL LATTICE MONTE CARLO METHOD

A. Basic description

In this kinetic 3D lattice Monte Carlo (K3DLMC) approach a homogeneous, chemically inert matrix is host of atoms of type A (the minority phase; quantitatively characterized by the volume fraction ϕ), which can be found either as dissolved monomers or as precipitated clusters. In our model the positions of the atoms are defined on a 3D lattice (we use the fcc lattice throughout this work) and for their kinetics effective NN interactions between A atoms are taken into account. This simplified effective-particle approach assumes that the A atoms are embedded in a position-independent potential of the substrate, which includes all the complex interactions between A and matrix atoms.

The thermodynamic properties are described with the help of the classical lattice gas model, i.e., in the framework of the NN Ising model.[40] Here, the Hamiltonian is given by $\mathcal{H}=-J\Sigma_{i<j}C_iC_j$, with occupation variables $C_i\in\{0,1\}$ and a bond strength $J>0$ effective only for NN pairs. Since any NN bond is shared by two atoms, the potential energy of a particular atom is given by $E_p=-nJ/2$. This implies a binding energy of a bulk atom $E_b=-\xi J/2$, where $\xi=12$ is the fcc coordination number.

The activation energy E_A denotes the diffusion barrier governing a single NN jump of an impurity atom. In our model both the matrix diffusion of a free monomer and the surface diffusion of an adatom on a precipitate surface are controlled by the same activation energy E_A.

Using the Metropolis algorithm,[41] the probability for an atom to jump from site i to an empty NN site f is

$$W_{if}=\begin{cases}\tau_0^{-1}\exp\{-E_A\beta\}, & n_f\geqslant n_i,\\ \tau_0^{-1}\exp\{-[E_A+(n_i-n_f)J]\beta\}, & n_f<n_i,\end{cases} \tag{2.1}$$

where $\Gamma_0=\tau_0^{-1}$ denotes the frequency of jump attempts, $n_{(i,f)}$ represents the number of NN bonds at the two sites, and $\beta=(k_BT)^{-1}$.

In order to reduce simulation time it is convenient to allow every diffusion attempt, i.e., $\tilde{W}_{if}=W_{if}/(\tau_0^{-1}\exp\{-E_A\beta\})$, which renormalizes just the time scale of the model. With the notation $\epsilon=J\beta$ this leads to the dimensionless transition probability

$$\tilde{W}_{if}=\min(1,\exp\{-(n_i-n_f)\epsilon\}), \tag{2.2}$$

and the quantity $\tau=\tau_0\exp\{E_A\beta\}$ defines the time scale of a MC step. In cases where $n_i>n_f$ holds (i.e., transitions, which are energetically not favored), the jumps are nevertheless allowed if a random number chosen from the interval $[0,1]$ is less than $\tilde{W}_{if}$.

In this work a MC step is defined by a sequence of N jump attempts of statistically independently chosen atoms out of the full set of N atoms. If for a single jump attempt the randomly determined NN site $\mathbf{r}_f$ is already occupied, another randomly chosen atom is checked for a possible jump.

Since each lattice site is completely defined by its occupation state, only a single bit is needed to represent each position. Thus the K3DLMC method can be implemented very efficiently on the basis of bit manipulations[42,43] in order to perform jump attempts of atoms, the core procedure of the code. Furthermore, using a double-bookkeeping strategy in bit and coordinate space to keep track of the positions of the impurities, this code (not parallelized) allows the simulation of reasonably sized systems on current top-level workstations.

Constructing our fcc lattice from an underlying simple cubic structure, our simulation cell has (100) symmetry. The lengths of the sides of the simulation cell are expressed in terms of the fcc lattice constant a, i.e., $L_i=2^{n_j}a$, $j\in\{x,y,z\}$. The discretization of the box volume in powers of 2 has advantages concerning the implementation of periodic boundary conditions.[40]

For the extraction of simulation data (mainly the size and space distribution of the nanoclusters) the whole simulation volume is scanned for the lattice positions of the atoms. For instance, if a lattice site is occupied, a recursive procedure checks all $\xi=12$ NN positions for further atoms. After the scan the numbers of monomers, dimers, trimers, . . . , or any agglomeration of interconnected atoms are known. Furthermore, the position of each nanocluster is calculated, which is defined as the center of mass of its atoms (with appropriate translations at periodic boundaries of the simulation box).

In this work the size of a cluster is given by the number i of atoms it consists of. This standard Ising droplet model is justified at low temperatures [T considerably below the intrinsic critical temperature T_c, i.e., ϵ considerably larger than $\epsilon_c=0.1021$ (Ref. 44)] and concentrations below the percolation threshold. Alternatively and more useful for the comparison of K3DLMC results to the LSW theory, the size of one (equilibrated) nanocluster is approximated by the radius of the smallest possible sphere which allows one to accommodate the number of its atoms on regular lattice sites. For a fcc lattice this relation is given by

$$\frac{4\pi}{3}R^3=iV_a=i\frac{a^3}{4},\quad i\gg 1, \tag{2.3}$$

where V_a denotes the atomic volume. However, the problem arises to define a lower limit i_l of nanocluster size, because a monomer can hardly be considered as a nanocluster. In this work the (arbitrary, temperature-independent) choice $i_l=6$ has been used.

It should be noted that this procedure of a spherical cluster approximation does a very poor job in the case of two coalescing precipitates. In this case the analysis of the radial inhomogeneity of a nanocluster helps to some extent to reveal its shape. For this purpose the normalized mean-square distance δ from the center of mass of the nanocluster has been introduced, which is defined as (analogous to the moment of inertia)

$$\delta=\frac{1}{R^2}\sum_{i=1}^{N_{NC}}(\mathbf{r}-\mathbf{r}_i)^2. \tag{2.4}$$

Here, R denotes the radius of the nanocluster [as determined by Eq. (2.3)], $\mathbf{r}$ is the center-of-mass coordinates of the cluster, and the summation is to be taken over all atoms connected to the cluster.

Recording δ for each nanocluster during the K3DLMC simulation provides a means to check, for instance, the relative contribution of coagulation to nanocluster coarsening. This can be done, because in the case of two touching precipitates the shape parameter δ considerably exceeds the value of an octahedral-like cluster,[45] which is the low-temperature equilibrium cluster shape on a fcc lattice.[46]

B. Gauging of simulation parameters

Modeling phase-separation phenomena by combined atomistic and mean-field simulations requires a well-defined interface between both methods. Therefore, the free simulation parameters of the model, i.e., the activation energy for diffusion E_A and the energy J of a NN bond between atoms, have to be defined in terms of macroscopic thermodynamic expressions.

The basic length scale of our K3DLMC model is the lattice constant a of the fcc lattice, on which the atoms diffuse and may condense to precipitates or form other kinds of nanostructures. For system-specific K3DLMC simulations the value of a is accessible by x-ray diffraction measurements at samples containing reasonably large nanoclusters or simply by taking tabulated bulk values.

1. Diffusion coefficient and time scale

The intrinsic diffusion coefficient of the K3DLMC method and the time scale τ of a MC step are coupled to the experimentally measured diffusion coefficient $D_{expt}=D_0\exp\{-E_A^{expt}(T)\beta\}$. The last expression assumes that cer-

tain temperature intervals exist, where diffusion is governed by a single activation energy $E_A^{expt}(T)$. Both D_{sim} and τ are derived within the framework of the random walk theory of diffusion (see, e.g., Ref. 47), which assumes independence of successive diffusion steps. The diffusion coefficient for particles on a lattice, which are only allowed to migrate to NN positions, is given by[47]

$$D_{latt}=\Gamma a^2/\xi, \tag{2.5}$$

where $\Gamma=\tau^{-1}$ is the effective jump frequency and $\xi=12$ denotes the corresponding coordination number of the fcc lattice. Note that the jump frequency is the product of the frequency of jump attempts Γ_0 times a temperature-dependent probability, i.e., $\Gamma=\Gamma_0\exp\{-E_A\beta\}$.

It is convenient in kinetic MC simulations to normalize the event with the highest probability to unity, which in the current model corresponds to allowing every possible (bulk or surface) diffusion attempt. This reduces the normalized K3DLMC diffusion coefficient to a purely geometric quantity, i.e., $D_{sim}=D_{latt}/\Gamma=a^2/\xi$.

With the help of the Einstein relation[47] the diffusion lengths are related by

$$\sqrt{2D_{expt}t}=x=\sqrt{2D_{latt}\tau k}=\sqrt{2D_{sim}k}, \tag{2.6}$$

where k denotes the number of MC steps. The last equation is valid in the asymptotic limit, i.e., for $k\to\infty$.

With the help of Eq. (2.6) the time constant τ or, equivalently, the jump frequency Γ can be obtained:

$$\tau=\frac{a^2/\xi}{D_0\exp\{-E_A^{expt}\beta\}}. \tag{2.7}$$

Thus, due to the temperature-dependent diffusion coefficient, one MC step can correspond to time intervals, which may differ by orders of magnitude. The total number of MC steps times the duration of a single MC step determines the physical time scale which can be modeled by the K3DLMC method, i.e., $t=\tau k$.

2. Nearest-neighbor bond strength and solubility

Within the framework of the lattice gas model the value of the NN bond strength J can be gauged by the solubility of the atoms in the matrix. In the following it is assumed that the solubility can be described (at least in a well-defined low-temperature regime) by an Arrhenius law $c_\infty=c_\infty^0\exp\{-E_S\beta\}$, where E_S is the activation energy for the dissolution of one monomer and c_∞^0 a temperature-independent constant.

The underlying idea is to determine the temperature-dependent concentration c of dissolved atoms which are in equilibrium with a flat interface of the bulk phase of this material. The initial setup for this simulation approach consists of a layer of atoms, which acts as the condensed phase.[48] If the layer extends from z_1 to z_2, its ''bulk'' behavior is achieved by keeping the atoms at $z=z_2$ fixed at their positions [see Fig. 1(a)]. Applying periodic boundary conditions in the x and y directions and preventing diffusion through the boundary at z_0, the minimization of the corresponding thermodynamic potential drives the evolution of the system. This particular setup represents a canonical ensemble (the simulation volume V, the number of atoms N, and the temperature ϵ are fixed); thus the free energy $F=U-TS$ will be minimized. It follows that both subsystems (i.e., the ''gas'' of dissolved monomers and the bulk phase) evolve under the constraint of maintaining equal chemical potentials, and thus phase equilibrium is obtained.

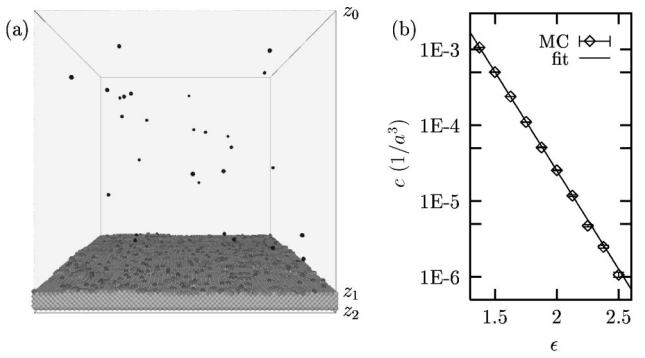

FIG. 1. Intrinsic solubility properties of the K3DLMC model. The snapshot of (a) obtained after 2×10^6 MC steps for $\epsilon=1.75$ indicates the simulation setup in (100) geometry. The Arrhenius plot in (b) shows the temperature dependence of the solubility of monomers.

In a series of simulations for different values of ϵ the averaged number of dissolved atoms[65] is determined after the configuration has reached equilibrium. For this purpose, the evolution of the system was followed for 4×10^6 MC steps. This period was divided into 500 equidistant time intervals, where at the end of each of the last 400 intervals the number of dissolved atoms was recorded. The corresponding averaged concentrations normalized with respect to the fcc unit cell are given in Fig. 1(b).

The relation between concentration and scaled temperature has been established with the help of the Arrhenius form

$$c_\infty(\epsilon)=A\exp\{-B\epsilon\}. \tag{2.8}$$

The fitted values of the constants read $A=(4.02\pm0.07)a^{-3}$ and $B=(5.99\pm0.01)$. The fitted slope B corresponds to half the fcc coordination number ($\xi=12$). Therefore, the total binding (i.e., sublimation) energy of a monomer $E_b=-BJ$ is equivalent to the activation energy $-E_S$ for its dissolution. This allows us to gauge the NN bond strength according to

$$J=2E_S/\xi, \tag{2.9}$$

which introduces an absolute temperature into the K3DLMC model. The last equation is expected to hold on other lattices (e.g., bcc or simple cubic lattices) as well, if the corresponding lattice coordination number ξ is adjusted properly.

Furthermore, we note that in the limit $T\to\infty$, the bulk density is reached, because the parameter A is equal to the number of atoms per fcc unit cell. The extrapolation towards $T\to\infty$ is only defined for temperatures below the intrinsic critical temperature T_c, which is usually above the physical melting or sublimation temperatures.

The nature of the coexistence of phases is defined by the thermodynamic properties of the interface. Since it is known that at a certain temperature $T_R \approx T_c/2$, there is a roughening phase transition from a smooth to a rough interface (with diverging interface correlation length; see, e.g., Refs. 49 and 50 and references therein); the above check of the principle of detailed balance is furthermore restricted to the regime $T < T_R$.

According to the critical temperature of the fcc kinetic Ising model in Fig. 1(b) the $c(T)$ phase diagram has been computed in the (normalized) temperature range $0.0408\ T_c < T < 0.0817\ T_c$ far below any critical phase transition. In this temperature regime physically reasonable solubility properties are observed. It should be noted that equilibrium conditions *independent* of the (100) phase boundaries have been achieved.

In order to apply the K3DLMC method for modeling the evolution of physically and technologically interesting systems (e.g., nanocluster formation of excess metallic or semiconducting impurity atoms in SiO_2) reliable values of the materials parameters have to be known. Taking the solubility as an example, typical values for the activation energy of dissolution are in the range $0.5\ \text{eV} \lesssim E_S \lesssim 3.0\ \text{eV}$. For instance, modeling a system characterized by $E_S = 1.0$ eV at 700 °C or 1000 °C, the corresponding scaled bond strengths read $\epsilon \approx 2$ and $\epsilon \approx 1.5$, respectively. Tabulated values of solubilities (c_∞^0, E_S) are usually the result of fits to measured data points within a restricted temperature regime. Therefore, values of c_∞^0 differing from the bulk density by orders of magnitude [e.g., the widely accepted solubility of Co in crystalline Si reads $c_\infty = 10^{26} \exp\{-(2.83\ \text{eV})\beta\}\ \text{cm}^{-3}$ (Ref. 51)] are not contradictory, but provide difficulties with respect to gauging of J in K3DLMC simulation approaches.

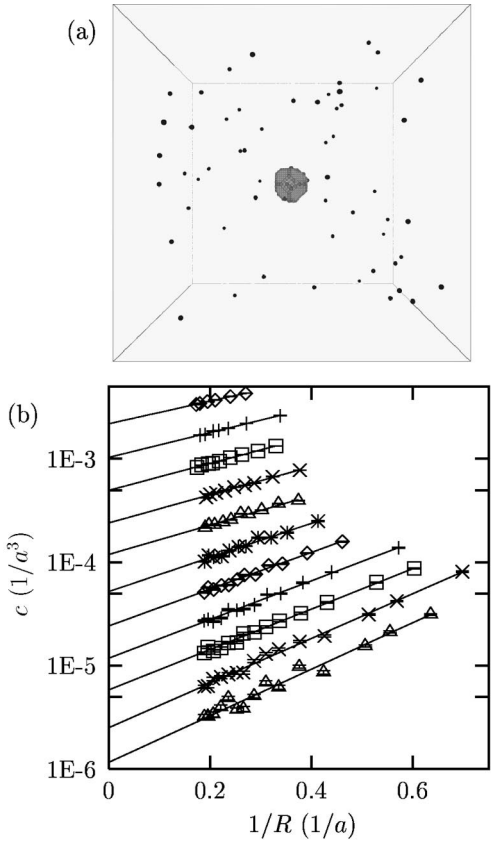

FIG. 2. In (a) the GT simulation setup (volume of simulation cell $(64a)^3$, periodic boundary conditions) is shown. In (b) MC simulation results are plotted (data points denote averages over 2×10^6 MC steps). From top ($\epsilon = 1.25$) to bottom ($\epsilon = 2.5$) the temperature has been changed in intervals of $\Delta\epsilon = 0.125$.

C. Intrinsic properties of the model

1. Gibbs-Thomson relation

A connection between atomistic and thermodynamic quantities is established by the Gibbs-Thomson (GT) relation, Eq. (2.10), which defines the equilibrium monomer concentration c around a spherical nanocluster of radius R:

$$c^{\mathrm{GT}}(R) = c_\infty \exp\left\{\frac{R_c}{R}\right\}, \quad R_c = 2\sigma V_a \beta. \tag{2.10}$$

The capillary length R_c is proportional to the surface tension σ.

In order to exploit Eq. (2.10) it has first to be shown that the K3DLMC method reproduces the GT relation. This has been done by a series of simulations, where a nanocluster of a specific size ("radius" R) is put in a simulation box of volume $V = 2^{n_x+n_y+n_z} a^3$ with $V^{1/3} \gg R$ [Fig. 2(a) shows the simulation setup]. Like in the case of the flat interface simulation, this highly artificial initial configuration will evolve at finite temperatures to a state with phase equilibrium between dissolved monomers and the *curved* bulk phase boundary (see also Ref. 52). For the analysis, averaged over a period of 2.5×10^6 MC steps [for the three highest values of ϵ in Fig. 2(b) the averaging was over 7.5×10^6 MC steps] the number of dissolved monomers is determined which are in equilibrium with this precipitate.[53,54] For the following analysis the radius of the nanocluster is derived according to Eq. (2.3).

Figure 2(b) shows the averaged simulated equilibrium monomer concentrations for several temperatures ϵ as a function of the cluster size. Two properties of the model can be deduced.

(i) The K3DLMC method excellently reproduces the GT relation even for very small nanoclusters.

(ii) By extrapolating for a given ϵ the GT relation to a flat interface (i.e., $R \to \infty$) the intersection of a fit with the y axis determines the solidus concentration.

Furthermore, by plotting the values of the solidus versus the simulation parameter ϵ [Fig. 3(a)] the solubility can be derived. Applying Eq. (2.8) to the simulation results one obtains $A^{\mathrm{GT}} = (3.64 \pm 0.08) a^{-3}$ and $B^{\mathrm{GT}} = (5.93 \pm 0.02)$, which is in good agreement with the results of the flat-interface analysis. While one could argue that the flat-interface simulations are influenced by the specific choice of (100) phase boundaries, the agreement of both simulation results is evidence that the interface orientation of the phase boundary does not effect intrinsic properties of the K3DLMC model.

It should be noted that the GT relation is supposed to be valid also for concave interfaces. For instance, the monomer

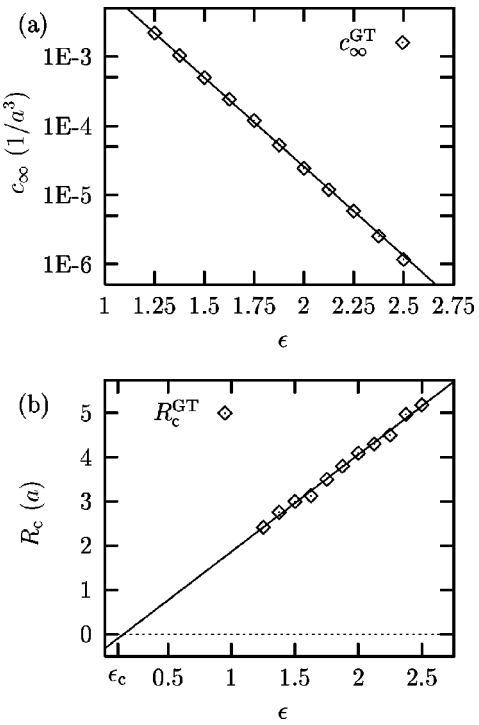

FIG. 3. In (a) the solubility properties are derived using results of the extrapolated solidus obtained by the GT simulations of Fig. 2. In (b) the fitted capillary lengths are plotted vs ϵ; the critical point of the fcc lattice is denoted by ϵ_c.

concentration in a spherical cavity of radius R within the bulk phase should be given by Eq. (2.10) after performing the transformation $R \rightarrow -R$ (see Fig. 4). In the particle picture, a positive (negative) curvature corresponds to a convex (concave) phase boundary. In the vacancy picture, the effective surface curvatures are reversed, i.e., convex $\leftrightarrow$ concave. Furthermore, due to the symmetry of the Ising Hamiltonian with respect to a particle-vacancy interchange [i.e., $C_i \rightarrow (1 - C_i)$],[66] the surface tension transforms appropriately. This particle-vacancy symmetry is reflected in the GT relation of Fig. 4. As an implication, the product of the averaged monomer and vacancy concentrations outside and within a nanocluster is constant, i.e., $cc_V = c_\infty^2$.

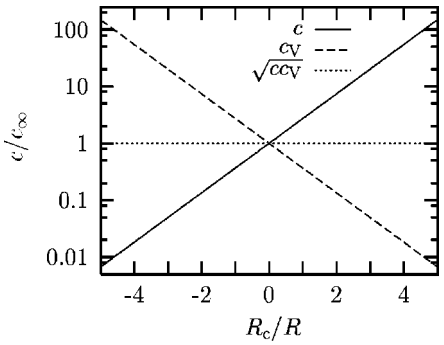

FIG. 4. Generalized GT relation of the Ising model relating the equilibrium monomer and vacancy concentrations c and c_V to convex and concave phase boundaries, respectively.

2. Capillary length and surface tension

A further analysis of the GT data allows us to derive explicit expressions for the capillary length R_c and the effective surface tension σ. Plotting the fitted capillary lengths R_c^{GT} versus the scaled bond strength ϵ [see Fig. 2(b)] a linear dependence is observed, i.e.,

$$R_c(\epsilon) = R_{c0} + \zeta a \epsilon. \tag{2.11}$$

According to the least-squares fit the constants are given by $R_{c0} = (-0.32 \pm 0.09)a$ and $\zeta = (2.19 \pm 0.05)$. The zero of the capillary length at a finite temperature (more precisely at $T = T_c$) is a prerequisite of the fact that the surface tension vanishes at the critical point.[55,56] This condition is reasonably satisfied by the *linear* extrapolation of the simulation results. However, close to the critical point the surface tension in lattice models is known to vanish like $\sigma \propto (1 - T/T_c)^{2\nu}$ with $\nu \neq 1/2$ [for instance, the critical exponent for the simple cubic lattice is known to be $\nu \approx 0.6$ (Ref. 56)].

According to the standard terminology σ denotes the interface free energy per unit area. Therefore, the surface tension cannot be obtained directly by counting the average number $\langle N_J \rangle$ of broken bonds of the cluster surface atoms and dividing this value by the mean (spherical) surface area $\langle S \rangle$. Having in mind that the surface tension is composed of an internal σ_I and entropic σ_E part (i.e., $\sigma = \sigma_I + \sigma_E$), this approach would just specify σ_I. The entropic part σ_E accounting for the number of different states in phase space is not accessible by this method.

With the help of the relation $R_c = 2\sigma V_a \beta = (2\sigma V_a / J)\epsilon$ [see Eq. (2.10)] for the capillary length, the surface tension is coupled to the NN bond strength J according to

$$\sigma = \frac{J}{2V_a \epsilon}(R_{c0} + \zeta a \epsilon) = \frac{2J}{a^2}\left(\frac{R_{c0}}{a\epsilon} + \zeta\right), \tag{2.12}$$

where $4V_a = a^3$ has been used. The last equation establishes a spherically averaged effective surface tension of a nanocluster, while usually macroscopically measured surface tensions are defined with respect to a specified interface orientation. Moreover, the temperature dependence of σ (at least in the simulated temperature regime) is given by Eq. (2.12), indicating a limiting value $\sigma \rightarrow \sigma_{T_0} = 2\zeta J/a^2$ for vanishing temperature. In comparison with the surface tensions of the principal fcc surfaces, σ_{T_0} is slightly larger than the zero-temperature value $\sigma_I(110) = 6/\sqrt{2}J/a^2$.

Within the framework of classical nucleation theory,[6–8] Eq. (2.12) can be used to calculate the critical size and the minimum reversible energy needed to form a cluster, given that the initial supersaturation is known.[45]

III. MESOSCOPIC MODELING OF OSTWALD RIPENING

A. Ostwald ripening: Basic theory

Here, a short summary of the LSW theory of OR is presented.[13,14] In their global mean-field theory an ensemble of nanoclusters is described by the time-dependent PRD function $f(R,t)$, where $f(R,t)dR$ denotes the number of par-

ticles per unit volume which have a radius between R and $R+dR$. Accordingly, the nanocluster density, normalized to unit volume, is given by $n(t)=\int f(R,t)dR$.

In the limiting case of a highly dilute system the precipitates are assumed not to interact directly. This implies that all clusters are embedded in the *same* average monomer concentration $\overline{c}$. In this case, the evolution of a single cluster (in the regime of diffusion controlled OR) is given by

$$\frac{dR}{dt}=-\frac{DV_a}{R}[\hat{c}(R)-\overline{c}]. \tag{3.1}$$

Here, $\hat{c}(R)$ denotes the equilibrium monomer concentration of a cluster of radius R, for which usually the GT relation is inserted. The mean concentration $\overline{c}$ is associated with a specific nanocluster radius $R^\star$, which can be expressed via the GT relation as a function of the solubility and capillary length. Since precipitates larger than $R^\star$ will grow, whereas those being smaller will shrink, this radius is called the critical radius of the ensemble. It should be noted that only in the case of diffusion-controlled OR, which we discuss here, does the relation $\langle R\rangle=R^\star$ hold.[14,28]

With the help of the linearized GT relation

$$c^{\mathrm{LSW}}(R)=c_\infty\left(1+\frac{R_c}{R}\right), \tag{3.2}$$

the single-cluster growth law, Eq. (3.1), can be rewritten as

$$\frac{dR}{dt}=-\frac{DV_a c_\infty R_c}{R^2}\left(1-\frac{R}{R^\star}\right). \tag{3.3}$$

Combining Eq. (3.3) with the continuity equation for f in size space and taking material conservation into account, LSW derived the following power laws for the critical radius and the cluster density (in the limit of diffusion control) (Ref. 13 and 14):

$$\langle R\rangle(t)=\langle R\rangle_0\left(1+\frac{t}{\tau_{\mathrm{diff}}}\right)^{1/3}, \tag{3.4}$$

$$n(t)\propto t^{-1} \quad \text{for} \quad t\gg\tau_{\mathrm{diff}}. \tag{3.5}$$

The characteristic time constant of diffusion-controlled OR is given by $\tau_{\mathrm{diff}}=9\langle R\rangle_0^3/(4c_\infty DV_a R_c)$, where $\langle R\rangle_0$ is the initial critical radius. Furthermore, the LSW theory predicts that the PRD, if scaled by the mean radius $\langle R\rangle(t)$, has a characteristic stationary form (see Refs. 13 and 14 for the corresponding analytical expressions).

For nonvanishing volume fractions the LSW theory is no longer strictly valid, because the long-range diffusion fields start to overlap. As a consequence, the monomer concentration around a nanocluster is now influenced by the presence of neighboring precipitates, which modifies the single-cluster growth law, Eq. (3.1). On the basis of extensive studies in the case $\phi>0$ it has been shown,[18,21,22] that the power laws, Eqs. (3.4) and (3.5), are still valid, whereas the characteristic time constant τ_{diff} and the PRD become a function of ϕ.

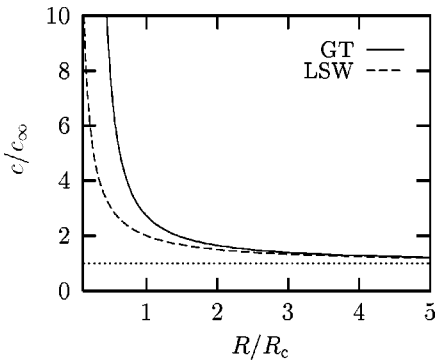

FIG. 5. Comparison of the equilibrium monomer concentration of a nanocluster of radius R according to the exact [Eq. (2.10)] and linearized [Eq. (3.2)] GT relations.

It should be stressed that the LSW theory is based on the linearization of the GT relation [see Eq. (3.2)]. Thus care has to be taken by applying the LSW theory to systems, where $\langle R\rangle\gg R_c$ is not valid. As Fig. 5 indicates, the exact GT relation gives much higher equilibrium concentrations for $R\lesssim R_c$, thus nanoclusters in this regime tend to dissolve more rapidly than the LSW theory predicts. Consequently, as will be shown below, nanocluster ensembles with $\langle R\rangle\lesssim R_c$ are governed by a (transient) dynamics, which may considerably differ from the LSW predictions, Eqs. (3.4) and (3.5).

B. Rate-equation simulation of Ostwald ripening

An appropriate framework for simulation studies of OR is a local mean-field description first derived by Voorhees and Glicksman (VG),[24,25] who treated the interacting precipitates as fixed-point-like sources characterized by a (fictitious) radius.

The starting point for this approach is to solve the stationary diffusion equation $\vec{\nabla}^2 c(\mathbf{r},t)=0$ defined in the multiply connected space outside the precipitated phase. The concentration field has to fulfill appropriate boundary conditions for the monomer concentration at each phase boundary $c(\mathbf{r})|_{|\mathbf{r}-\mathbf{r}_i|=R_i}=\hat{c}_i$ and additionally $\lim_{|\mathbf{r}|\to\infty}c(\mathbf{r})=c_u$. Considering the characteristic time scales one generally loses no information in neglecting the time derivative of the diffusion equation. This is due to the fact that the time scale involved in the precipitate growth is usually much larger than that of the diffusional accommodation of the monomer concentration to the existing precipitate pattern.

The concentration field can be expressed as a sum over multipole expansions,

$$c(\mathbf{r})=c_u+\frac{1}{4\pi D}\sum_{i=1}^{N}\sum_{l=0}^{\infty}\sum_{m=-l}^{l}\frac{Y_l^m(\theta_i,\phi_i)M_{il}^m}{|\mathbf{r}-\mathbf{r}_i|^{l+1}}, \tag{3.6}$$

using the common notation Y_l^m to denote the spherical harmonics. The multipole moments M_{il}^m, which take into account the diffusional nanocluster interaction, can be obtained

by integration over the (spherical) surface of the ith precipitate using the orthogonal properties of the spherical harmonics involved.

In this approach, like in the original VG model,[24,25] OR is described on the basis of the monopole approximation of Eq. (3.6), which is a reasonable approximation for small volume fractions [$\phi<0.1$ (Ref. 57)] of the minority phase. Recently, more advanced approaches included higher-order (dipole, ...) terms of nanocluster interaction, which account for migration and spherical shape deviations of precipitates.[58,27]

In the monopole approximation the source strengths $Q_i = Y_0^0 M_{i0}^0$ can be obtained from a linear system of equations

$$Q_i = 4\pi D R_i \left[\hat{c}(R_i) - \frac{1}{4\pi D} \sum_{j \neq i}^{N} \frac{Q_j}{|\mathbf{r}_i - \mathbf{r}_j|} - c_\mathrm{u} \right]. \quad (3.7)$$

Please note that the last expression has been derived in the limit of diffusion-controlled ripening, whereas, more generally, the source strengths can be obtained for any degree of diffusion or reaction control.[29,30] Additionally, for studies of homogeneous OR one usually assumes material conservation, i.e., $\Sigma_i Q_i = 0$, which fixes the value of the free parameter c_u. In order to avoid boundary effects in studies of homogeneous OR, a three-dimensional periodic extension of the nanocluster ensemble is considered. In this case, the source strengths are computed with the help of Ewald summation.

The individual source strengths Q_i determine the evolution of the precipitates:

$$\frac{4\pi}{V_\mathrm{a}} R_i^2(t) \frac{\mathrm{d}R_i(t)}{\mathrm{d}t} = -Q_i. \quad (3.8)$$

Equation (3.8) and the diffusion equation form a coupled system of differential equations controlling the evolution of the precipitates.

The local mean-field character of this approach is clearly seen in Eq. (3.7), since the source strength of the ith precipitate is proportional to the difference between its own equilibrium concentration and the superposition of the resulting mean concentration c_u and the concentration fields caused by all other nanoclusters. The evolution of individual precipitates is mainly determined by the diagonal elements of Eq. (3.7), whereas the off-diagonal elements account for the coupling of nanoclusters. It should be noted that in the limit $\phi \to 0$, i.e., $|\mathbf{r}_i - \mathbf{r}_j| \to \infty$, the LSW growth law, Eq. (3.1), for a single precipitate is obtained.

While the linearization of the GT relation is an essential ingredient of the LSW theory, in the numerical model either the linearized or exact form can be used for the implementation of Eq. (3.7). In the former case all physical quantities can be absorbed into the time scale; thus OR is only dependent on the geometry, i.e., on the coordinates $\{\mathbf{r}_i\}$ and radii $\{R_i\}$ of the nanoclusters. Using Eq. (2.10) in order to compute the equilibrium monomer concentration of the nanoclusters, the evolution of an ensemble of nanoclusters will in general depend on the capillary length, more precisely on the ratio $R_\mathrm{c}/R^\star(t)$.

The rate-equation approach needs as essential input the coordinates $\{\mathbf{r}_i\}$ and radii $\{R_i\}$ of the nanoclusters. Taking into account statistical properties of nanocluster ensembles (e.g., spatial correlations and size distributions) the input data can be generated artificially. However, a more promising option is to use data sets obtained from a subsequent K3DLMC simulation.[53]

The simulation is discrete in time; i.e., at each time step Δt, first the linear system of equations (3.7) extended by one equation fixing c_u is solved. Then the change in radius due to the actual value of the source strengths is evaluated with the help of a linear approximation of Eq. (3.8). With the new radii obtained the procedure is repeated. The time interval Δt can be chosen to some extent arbitrarily as long as material conservation is not violated.[59]

At the end of this section we would like to make a comment concerning finite-size effects, since in the course of an OR simulation run the density of clusters decreases. Within an ensemble of nanoclusters, the diffusional screening length[60]

$$\lambda_\mathrm{D}(t) = \frac{1}{\sqrt{4\pi n(t) \langle R \rangle(t)}} \quad (3.9)$$

defines the length scale of nanocluster interactions. Since a monomer detaching from a nanoclusters is very likely to migrate to a nearby precipitate on his random walk, λ_D denotes the distance beyond which the diffusional interaction is screened by the remaining ensemble a nanocluster is embedded in. Thus the OR simulations have to be checked that self-interactions of nanoclusters are avoided in cases where periodic boundary conditions are applied.

IV. SIMULATION RESULTS AND DISCUSSION

A. Monte Carlo simulations of homogeneous Ostwald ripening

1. Conventional coarsening analysis

In order to analyze the properties of the K3DLMC model with respect to OR, in a series of simulations on a fcc lattice systems with volume fractions $\phi = 0.01$ have been studied. We used a system size of $V = (128\,a)^3$ and applied periodic boundary conditions. Starting with instantaneous high-temperature quenches to five different temperatures (namely, $\epsilon \in \{1.25, 1.5, 1.75, 2.0, 2, 25\}$) the evolution of the atoms has been monitored over a period of 4×10^6 MC steps.

Figure 6 shows the evolution of the nanocluster density $n(t)$ and the mean radius $\langle R \rangle(t)$. In these plots for each value of ϵ the average of five independent runs has been used. Size-dependent effects should not have influenced these simulations, since the largest diffusional screening length of this series [as obtained by Eq. (3.9)] for $\epsilon = 1.25$ is $\lambda_\mathrm{D} \approx 42a$. This value is considerably below the linear dimension of the simulation volume; thus self-interaction effects are negligible.

Care has to be taken in order to extract the growth behavior, since a fit assuming $\langle R \rangle \propto t^m$ is only justified for late times of phase separation. According to Eq. (3.4) this implies that the analysis should start at times $t \gg \tau_\mathrm{diff}$ from which the

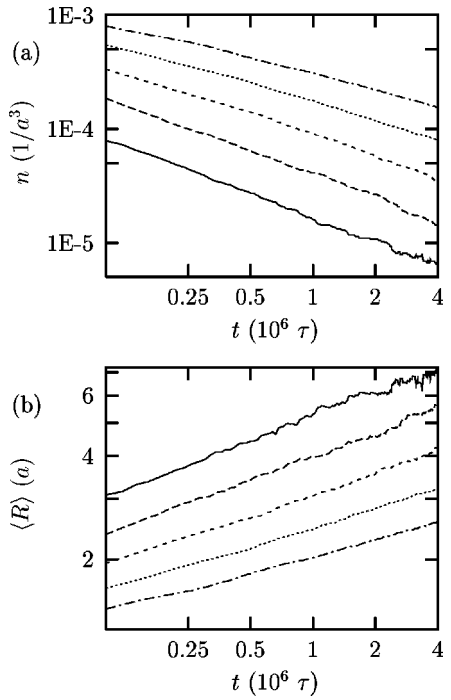

FIG. 6. Using double-logarithmic scales the evolution of the density of nanoclusters and of the mean radius are shown in (a) and (b), respectively. In the ln(n)-ln(t) plot, from bottom to top the curves correspond to $\epsilon=\{1.25,1.5,1.75,2.0,2.25\}$, whereas the reversed order is valid in the ln($\langle R\rangle$)-ln(t) plot.

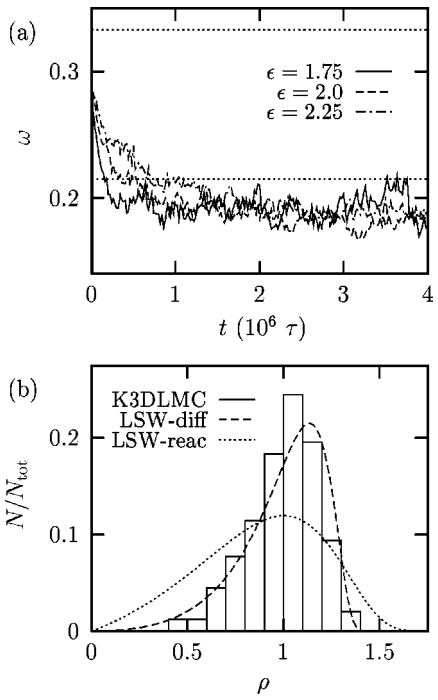

FIG. 7. In (a) the evolution of the widths ω of PRD's corresponding to the simulations for the three lowest temperatures of Fig. 6 are shown. As a reference the widths of both the limiting distributions of the LSW theory (Refs. 13 and 14) are added, which read $\omega_{\rm diff}=0.215$ and $\omega_{\rm reac}=0.333$, respectively. In (b) a histogram of the PRD of a single run for $\epsilon=2$ obtained after 2×10^6 MC steps is shown (with $\rho=R/\langle R\rangle$; both stationary PRD's of the LSW theory have been added).

relation $\langle R\rangle(t)\gg\langle R\rangle_0$ follows. Due to the quench, the initial system consisted entirely of monomers; thus for an application of the LSW theory the mean radius has to be large with respect to $R_0\approx0.39a$. Assuming that this requirement is fulfilled (at least in the end of the simulations), least-squares fits performed in the time interval $1\times10^6<t<4\times10^6$ MC steps yield growth exponents $m(\epsilon=1.25)=0.19$, $m(\epsilon=1.5)=0.26$, $m(\epsilon=1.75)=0.23$, $m(\epsilon=2.0)=0.19$, and $m(\epsilon=2.25)=0.17$, respectively. These results would indicate a temperature dependence of ripening (the data for $\epsilon=1.25$ show a very bad statistics), which is not predicted in the LSW theory [Eq. (3.4)].

More insight into the dynamics of the K3DLMC method is gained by plotting the widths of the PRDs, defined as

$$\omega(t)=\sqrt{\langle[R/\langle R\rangle(t)-1]^2\rangle}, \tag{4.1}$$

as can be seen in Fig. 7(a). Figure 7(b) shows the PRD for $\epsilon=2$ obtained after 2×10^6 MC steps. While the size distribution is in reasonable accordance with the stationary form (LSW) of the PRD of diffusion-limited OR, it is on the average somewhat smaller and seems to be more symmetric. Since the quasistationary form of the PRD is directly coupled to the growth law, the on-the-average smaller width ω as compared to the result of the diffusion-controlled LSW regime is in line with the observation $m<1/3$. But how can the observed OR behavior be explained consistently?

2. Effective growth exponent

A more careful analysis reveals that the simulated coarsening data cannot be analyzed in the framework of the standard LSW theory, because Eq. (3.3) is based on the linearization of the GT equation [i.e., use of Eq. (3.2) rather than Eq. (2.10); see also Fig. 5]. This is, however, not justified for the rather small nanoclusters of the current simulations, which becomes obvious by comparing the range of the mean nanocluster radius $\langle R\rangle$, as obtained by the simulations, to the corresponding capillary lengths. According to Eq. (2.11) the capillary length varies between $R_c(\epsilon=1.25)\approx2.42a$ and $R_c(\epsilon=2.25)\approx4.61a$. Thus for the lowest temperature of the simulation series ($\epsilon=2.25$), the mean domain size has only grown up to the order of the capillary length, whereas for the highest temperature ($\epsilon=1.25$) the ratio $R_c/\langle R\rangle$ has become small at the end of the simulation; a linearization of the GT relation would be justified in modeling this ensemble at *later* times.

Since in all simulations of this series the LSW requirement $R_c/\langle R\rangle\ll1$ is not satisfied, coarsening should be analyzed with respect to an effective growth exponent according to the growth law $\langle R\rangle(t)=A+Bt^{1/3}$. This approach has been motivated by domain growth studies in the two-dimensional case.[33,34] Without discussing the capillary length of the square lattice, these authors proposed an effective growth exponent

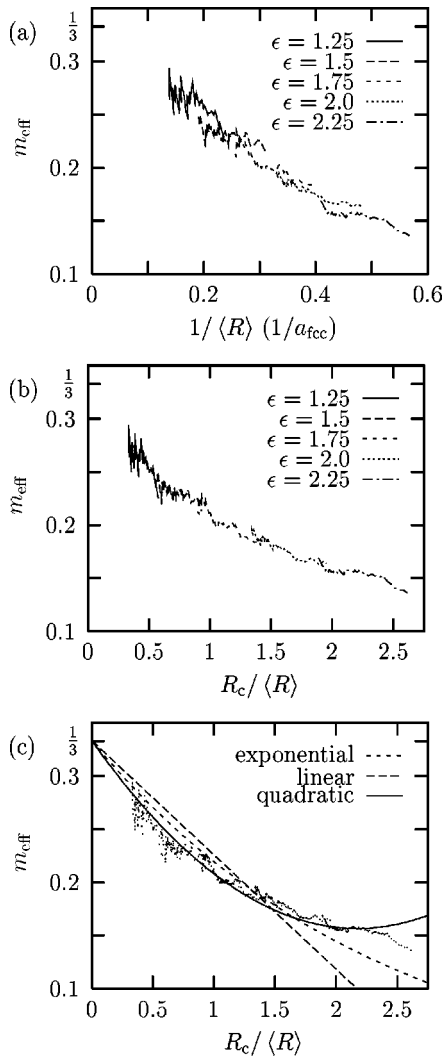

FIG. 8. Effective domain growth exponents $m_{\rm eff}$ of the K3DLMC model for $\kappa=4$ with data points in the range $t\geqslant 5\times 10^5$ MC steps. (a) Simulation results based on Eq. (4.2). (b) Replot of $m_{\rm eff}$ as a function of the dimensionless parameter $R_c/\langle R\rangle$. (c) Exponential as well as linear and quadratic fits according to Eq. (4.3).

$$m_{\rm eff}=\frac{1}{3}-\frac{C}{\langle R\rangle(t)}:=\frac{d\{\ln[\langle R\rangle(t)]\}}{d[\ln(t)]}. \tag{4.2}$$

Thus an analysis of the growth behavior has been performed using an appropriate implementation of Eq. (4.2), i.e., $m_{\rm eff}(t_f)=\ln[\langle R\rangle(t_f)/\langle R\rangle(t_i)]/\ln(t_f/t_i)$ with $t_f/t_i=\kappa$. The value of κ is not predefined; it should be chosen in a way to exclude fluctuations, but guarantee ''local'' time in this discrete implementation of the derivative of Eq. (4.2).[34] Figure 8(a) shows the results of the corresponding analysis for $\kappa=4$. Although there is an unequivocal trend towards the value $m(\langle R\rangle\rightarrow\infty)=1/3$, unfortunately the large scatter in the data can only provide evidence for this limiting theoretical value. Please note that the scatter in the data qualitatively remains unchanged in the tested regime $\kappa\in\{2,3,4,5,6\}$.

Obviously a good statistics is needed in order to obtain a smooth dependence of $\langle R\rangle$ on t (Amar *et al.*[34] used 100 independent runs in their study of the two-dimensional case). In the present study, however, averaging over five independent runs per temperature ϵ does not even provide a monotonically increasing mean cluster size.

Having a closer look on Fig. 8(a) one observes that the effective growth exponents seem to depend on temperature, i.e., do not tend to converge onto a single curve. More precisely, for a given mean cluster size $\langle R\rangle_0$, the larger the temperature T, the larger is the exponent $m_{\rm eff}$. This temperature behavior is similar to that of the inverse capillary length, so it is tempting to assume $C\propto R_c$. In Fig. 8(b) the effective growth exponents are replotted as a function of $R_c/\langle R\rangle$. Two features can be observed: (i) Despite the considerable scatter in the available data all points seem to converge onto a single curve; (ii) the effective growth exponent has a nonlinear dependence on $R_c/\langle R\rangle$ in the computationally explored regime $R_c/\langle R\rangle\gtrsim 1/2$.

At a first glance, the dependence of $m_{\rm eff}$ on $R_c/\langle R\rangle$ looks like an exponential decay. However, a fit according to $m_{\rm eff}=1/3\exp\{-C'(R_c/\langle R\rangle)\}$ provides only a very poor approximation, only slightly better than a linear fit [see Fig. 8(c)]. Therefore, using the notation $\tilde{C}_i=C_i/R_c^i$ and $\tilde{R}_i=[\langle R\rangle/R_c]^i$, the effective growth exponent is approximated as

$$m_{\rm eff}=\frac{1}{3}-\sum_{i=1}^{M}\frac{\tilde{C}_i}{[\tilde{R}(t)]_i}. \tag{4.3}$$

Figure 8(c) shows the result of a least-squares fit to the data using Eq. (4.3) up to second order ($M=2$). Obviously, a much better accordance is obtained as compared to a linear model. However, this attempt resulted in a coefficient $\tilde{C}_2<0$ which would indicate the existence of a minimum of the effective growth exponent. This is not supported by the current data nor is there any physical reason known to the authors assuming such a behavior.

Nevertheless, it would be of interest to study the dynamics of coarsening at very low temperatures, i.e., in the regime $R_c/\langle R\rangle\gg 1$. Such large values can be extrapolated because in this regime R_c is roughly proportional to $1/T$ [see Eq. (2.11)] and the stable cluster size decreases with decreasing temperature (with a dimer as the logical lower bound). At least as long as the GT relation [Eq. (2.10)] describes correctly the equilibrium monomer concentration of a cluster, the dynamic growth exponent can be expected to decrease further with an increasing value of $R_c/\langle R\rangle$.

In conclusion, Figs. 8(b) and 8(c) provide evidence that the effective growth exponent is a unique function of the ratio $R_c/\langle R\rangle$. In reverse, this means that a measure of $m_{\rm eff}$ in a homogeneous system of diffusively interacting nanoclusters provides some hint onto the value of the capillary length. For instance, from a value $m_{\rm eff}\approx 0.2$ it follows (see Fig. 8) that the mean size of the clusters is approximately equal to the value of R_c. Furthermore, in this regime characteristic PRD's are on the average smaller and more symmetric than the corresponding LSW-PRD of the diffusion limited case (see Fig. 7).

In addition to further theoretical efforts more simulation data are needed to address such questions as (i) the behavior of m_{eff} in the regime $R_c/\langle R\rangle > 1$ and (ii) the physical interpretation of the constant C_1/R_c in the limit $R_c/\langle R\rangle \to 0$. This temperature-independent quantity might have the meaning of a geometrical constant. Similar simulations in other dimensions, and their consistent interpretation, could help to clarify this conjecture.

3. Discussion of alternative phase-separation models

Although the dependence of the effective coarsening dynamics on the ratio $R_c/\langle R\rangle$ seems to offer a reasonable explanation for the observed growth exponents, there might be additional factors influencing the system evolution. Since the K3DLMC method automatically includes the migration of nanoclusters, it is tempting to analyze, if the nanocluster dynamics can be brought into accordance with the Binder-Stauffer theory of cluster growth.[61–63] In their model the cluster evolution proceeds mainly via coagulation rather than monomer evaporation and condensation. Therefore, coarsening occurs via coalescence of diffusing nanoclusters and is thus determined by the effective diffusion coefficient $D_{\mathrm{NC}}(i)$ of nanoclusters. Depending on the detailed atomistic mechanism by which the center of mass of a nanocluster moves (e.g., surface diffusion, diffusion of a vacancy within the nanocluster or evaporation of a monomer and recondensation at a different surface site), a growth law is derived, which in three dimensions varies between the regimes $\langle R\rangle \propto t^{1/6}$, $\langle R\rangle \propto t^{1/5}$, and $\langle R\rangle \propto t^{1/4}$, respectively. For instance, Toral and Marro[64] interpreted the change of the evolution of the normalized excess energy, $\Delta E/J \propto \langle R\rangle^{-1}$ (which is proportional to the surface energy, i.e., the driving force for coarsening), from a $m=1/6$ to a $m=1/3$ growth regime with a change from the cluster coagulation to the OR coarsening mechanism.

In order to prove whether this cluster growth mode influences the observed time dependences, the K3DLMC results have to be checked for the motion of nanoclusters and for deviations from the quasiequilibrated shape of faceted octahedras due to coalescence events. This is done by measuring in intervals of $\Delta t = 5000\,\tau$ the minimum distance between any two precipitates defined as $d_{\mathrm{min}} = |\mathbf{r}_i - \mathbf{r}_j|_{\mathrm{min}} - R_i - R_j$. As the plateaulike behavior of d_{min} in Fig. 9(a) indicates, no evidence for diffusional encounters of nanoclusters can be detected. Furthermore, the minimum observed distance of approximately $5a$ is larger than the maximum analyzed cluster diffusion length $\Delta r_{\mathrm{max}} \approx 4a$ for the whole coarsening process [the topic of cluster diffusion will be discussed in more detail below; see also Fig. 12(b)]. The slightly negative slope of the plateaus is not necessarily due to nanocluster diffusion; also nanocluster growth (see definition of d_{min}) can explain this observation. Consequently, in the recorded data of the nanocluster shape parameter δ [Eq. (2.4)] no significant deviations can be observed except for the smallest nanoclusters shortly to their dissolution [see Fig. 9(b)]. Thus it can be concluded that in the studied system cluster coagulation did not influence the coarsening dynamics.

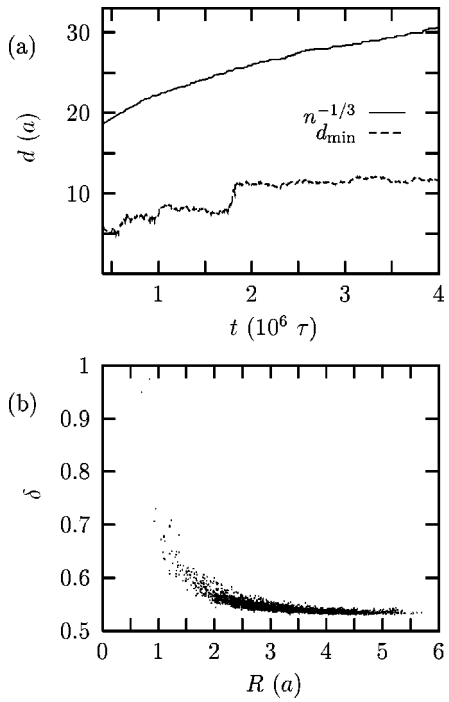

FIG. 9. In (a) the evolution of the mean nanocluster distance given by the inverse cubic root of the density is compared to the minimum nanocluster distance in the ensemble. In (b) the spectrum of the nanocluster shape parameter δ during OR ($4\times10^5\tau < t < 4\times10^6\tau$), as recorded every 2×10^5 MC steps, is plotted.

B. Comparison of K3DLMC and mean-field simulations of Ostwald ripening

The mean-field approach to OR verifies the LSW predictions provided that $R_c/\langle R\rangle \gg 1$ holds,[25,29] thus it is interesting to apply the mean-field method to systems characterized by $R_c/\langle R\rangle \approx \mathcal{O}(1)$. The direct comparison to the K3DLMC method reveals, furthermore, the similarities and differences of the atomistic and thermodynamic descriptions of domain growth.

Therefore, after a K3DLMC run over 4×10^5 MC steps of a system quenched to $\epsilon = 1.75$, the further evolution of the nanocluster ensemble was followed also in parallel with the mean-field description in the diffusion controlled regime (see Sec. III). This has been done by using geometrical data (i.e., the positions $\{\mathbf{r}_i\}$ and sizes $\{R_i\}$ of the nanoclusters) obtained from the K3DLMC simulation as input for the mean-field simulation. Please note that in order to do this data transfer a physically reasonable (but arbitrary value) has been assigned to the MC lattice constant a. While it is obviously necessary to choose in both methods the same value for R_c the actual value of the remaining materials parameters (solubility and diffusion coefficient) influences essentially only the absolute time scale of OR.

Figure 10 shows the corresponding results after 3.6×10^6 MC steps. At a first glance both simulation results seem to be very similar. This becomes obvious by comparing Figs. 10 (b′) and 10 (c′), the respective spherical cluster representations of the K3DLMC simulation, with the corresponding mean-field simulation results shown in Figs. 10(d)

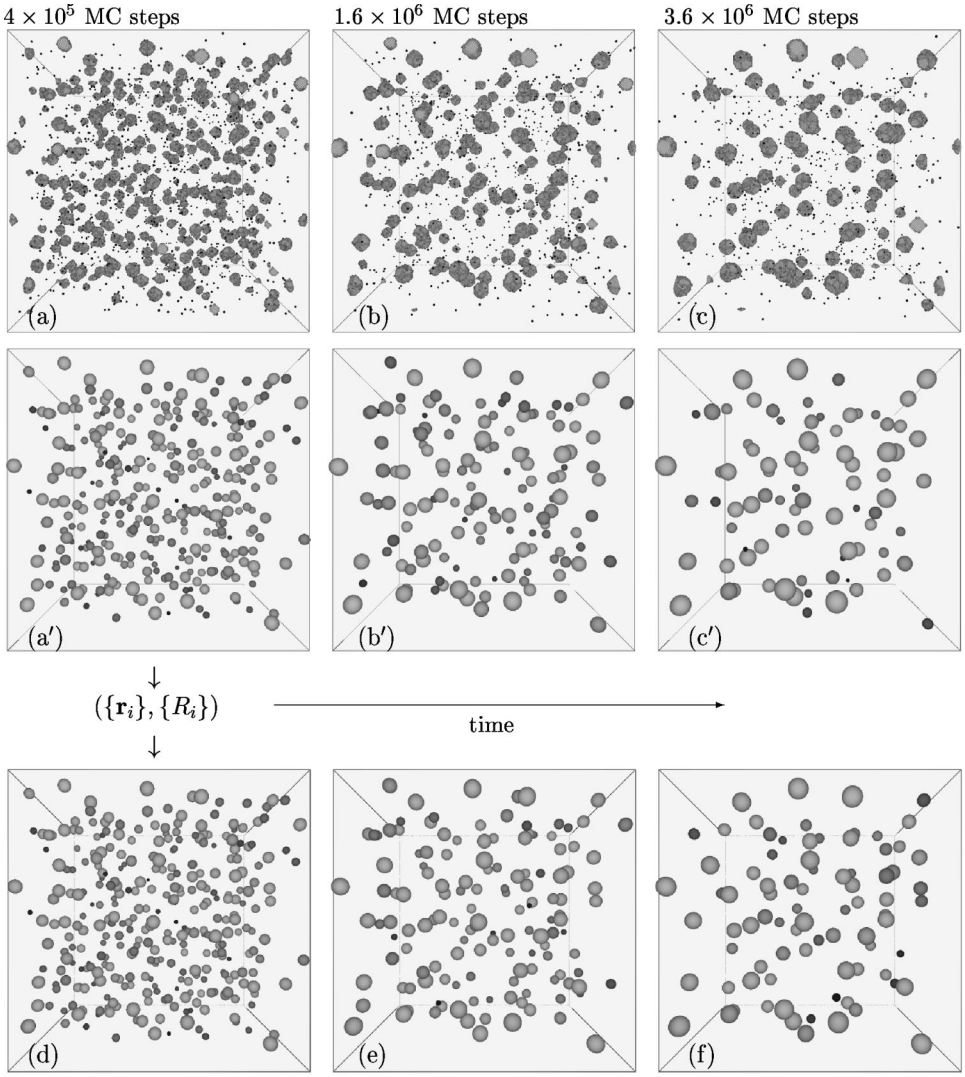

FIG. 10. Comparison of OR simulations with K3DLMC and mean-field methods of a fcc system with volume fraction $\phi = 0.01$ quenched to $\epsilon = 1.75$. Upper row [panels (a)–(c)]: snapshots from the K3DLMC simulation. Middle row [panels (a′)–(c′)]: the corresponding spherical cluster representation. The mean-field (MF) simulation starts with K3DLMC input data as recorded at $t = 4 \times 10^5$ MC steps. Lower row [panels (d)–(f)]: the ensemble is shown at equal nanocluster densities, i.e., $n_{\mathrm{MF}} = n_{\mathrm{MC}}$.

and 10(f). However, a closer inspection reveals certain differences of the microscopic evolution (positions and sizes of remaining nanoclusters), which will be discussed below.

In order to compare the dynamics of both simulation methods, Fig. 11 shows the evolution of the nanocluster densities, which obey a quite similar behavior. For this comparison the absolute time scales of coarsening have been normalized properly by multiplicative factors. Noting that the mean cluster size is coupled to the cluster density via material conservation, it can be concluded that the effective growth exponents seem to be in accordance. In contrast, the additional plot of $n(t)$ obtained by the mean-field method using the linearized GT equation [LSW approximation, Eq. (3.2)] is clearly governed by a different exponent. This exhibits the influence of the choice of the driving force on the dynamics of OR.

The differences in the dynamics of both mean-field simulations is also reflected in the absolute time scales of coarsening. For the particular comparison presented in Fig. 11 the durations of ripening (measured in units of τ_{diff}) are related by $\Delta t_{\mathrm{LSW}} \approx 3 \Delta t_{\mathrm{GT}}$. In general, this time difference is a function of the ratios $R_c/\langle R \rangle_i$ and $R_c/\langle R \rangle_f$ for the initial and final mean radii and vanishes for $R_c/\langle R \rangle \to 0$. Since the K3DLMC method excellently reproduces the GT relation (see Fig. 2), it is obvious that a parallel or subsequent mean-

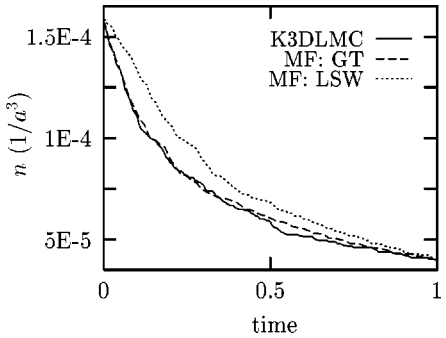

FIG. 11. Comparison of the evolution of the density of nanoclusters obtained by the K3DLMC and mean-field (MF) methods in the normalized time interval between $t_i = 4 \times 10^5\ \tau$ and $t_f = 3.6 \times 10^6\ \tau$ (see Fig. 9). The coarsening times of the MF simulations have been scaled with respect to the K3DLMC nanocluster densities at both t_i and t_f.

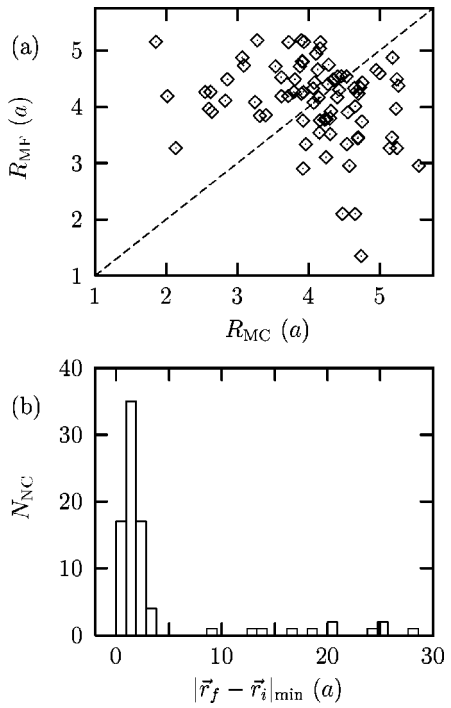

FIG. 12. Comparison of the evolution of nanoclusters obtained by the K3DLMC and mean-field (with GT) methods. In (a) the radii as obtained by both methods are directly compared. In (b) for each remaining nanocluster of the K3DLMC ensemble the distance to the nearest remaining nanocluster of the mean-field ensemble is determined.

field simulation should be based on an implementation of the exact GT relation rather than the LSW approximation (which ensures identical dynamical descriptions).

As already pointed out, a more detailed analysis reveals, that the sequence of dissolving nanoclusters depends on the simulation approach. Figure 12(a) shows the differences of the evolution of the ensemble in the parallel treatments by directly comparing the nanocluster sizes. While all data points would lie on a single line with unit slope in the case of identical evolutions, the scattered data indicate the differing evolution of individual nanoclusters in both methods. These differences with respect to the detailed evolution within each simulation method are not really surprising, because the mean-field simulation is deterministic once the input data $(\{\mathbf{r}_i\},\{R_i\})$ have been fixed, while the K3DLMC simulation is stochastic in nature. In particular, statistical fluctuations in the atomistic model can influence the growth behavior of a single nanocluster.

A further analysis with respect to the movement of nanoclusters inherently included in the K3DLMC method is shown in Fig. 12(b). In this plot for each surviving nanocluster of the MC simulation the nearest remaining nanocluster in the mean-field simulation is determined (note that the monopole approximation used in the mean-field method does not allow for nanocluster diffusion;[27] they remain fixed at their positions). While a majority of the nanoclusters has moved at most $\Delta r = |\mathbf{r}_f - \mathbf{r}_i| \approx 4a$, the few with no close remaining counterpart can easily be explained by the difference in the sequence of nanocluster dissolution of both descriptions. In particular, if nanocluster diffusion and coagulation would have dominated the coarsening kinetics (see discussion above), a different distribution of cluster diffusion lengths would have been expected.

In conclusion, despite model-specific differences in the detailed evolution both the atomistic and mean-field models describe the same overall domain-growth dynamics. With respect to the movement of nanoclusters observed in the K3DLMC it would be interesting to check the range of nanoclusters diffusion of corresponding mean-field approaches extended to the dipole approximation (which take into account nanocluster migration as well as shape deviation).[27]

V. SUMMARY

A kinetic 3D lattice Monte Carlo model with nearest-neighbor interactions and a mean-field model have been used to study coarsening of a diluted system of nanoclusters. It has been shown that knowledge of the capillary length R_c, consistently derived with in the Monte Carlo model, is essential for understanding and correctly interpreting the dynamics of domain growth. Moreover, evidence has been presented that the effective growth exponent is a unique function of the ratio $R_c/\langle R\rangle$. In a comparative study it has been shown that both the atomistic and mean-field simulation models result in the same cluster dynamics, provided the same driving forces are applied [use of the appropriate (i.e., exact or linearized) Gibbs-Thomson relation in the mean-field approach]. This also implies that the kinetic lattice Monte Carlo method would model the late stage of phase separation according to the Lifshitz-Slyozov-Wagner predictions if the computation power would allow for long-lasting simulations. The differences in the detailed evolution of one system in both models have been discussed in terms of the stochastic and deterministic nature of both approaches. Having shown that a well-defined interface exists between both models, in a hierarchical approach future multiscale simulations in materials science of phase-separating systems can use consistently the power of both the atomistic and mean-field descriptions.

ACKNOWLEDGMENT

We would like to thank the Central Computing Facilities of the Forschungszentrum Rossendorf for continuous support.

*Present address: PSI AG, Boschstr. 6, D-63741, Aschaffenburg, Germany. Electronic mail: strobel@fz-rossendorf.de

[1] C. Flytzanis, F. Hache, M. C. Klein, D. Ricard, and Ph. Roussignol, in *Semiconductor and Metal Crystallites in Dielectrics*, edited by E. Wolf (Elsevier Science, Amsterdam, 1991), p. 321.

[2] H.I. Hanafi S. Tiwari, and I. Khan, IEEE Trans. Electron Devices

43, 1553 (1996).
[3] P. Mazzoldi, G.W. Arnold, G. Battaglin, R. Bertoncello, and F. Gonella, Nucl. Instrum. Methods Phys. Res. B **91**, 478 (1994).
[4] C.W. White, J.D. Budai, J.G. Zhu, S.P. Withrow, R.A. Zuhr, Y. Chen, D.M. Hembree, Jr., R.H. Magruder, and D.O. Henderson, in Microcrystalline and Nanocrystalline Semiconductors, edited by L. Brus *et al.*, Mat. Res. Soc. Symp. Proc., Vol. 358 (Materials Research Society, Pittsburgh, 1995), p. 169.
[5] M. Strobel, K.-H. Heinig, and W. Möller, in *Ion Beam Synthesis and Processing of Advanced Materials*, edited by D. B. Poker, S. C. Moss, and K.-H. Heinig, Mat. Res. Soc. Symp. Proc., Vol. 647 (Materials Research Society, Pittsburgh, 2001), p. 23.
[6] M. Volmer and A. Weber, Z. Phys. Chem. (Leipzig) **119**, 277 (1926).
[7] R. Becker and W. Döring, Ann. Phys. (N.Y.) **24**, 719 (1935).
[8] D.T. Wu, Solid State Phys. **50**, 38 (1997).
[9] J. D. Gunton, M. San Miguel, and P. S. Sahni, in *The Dynamics of First-Order Phase Transitions*, edited by C. Domb and J.L. Lebowitz (Academic Press, London, 1983), Vol. 8, p. 267.
[10] J.L. Lebowitz, J. Marro, and M.H. Kalos, Acta Metall. **30**, 297 (1982).
[11] M.H. Kalos, J.L. Lebowitz, O. Penrose, and A. Sur, J. Stat. Phys. **18**, 39 (1978).
[12] O. Penrose, J.L. Lebowitz, J. Marro, M.H. Kalos, and J. Tobochnik, J. Stat. Phys. **34**, 399 (1984).
[13] I.M. Lifshitz, and V.V. Slyozov, J. Phys. Chem. Solids **19**, 35 (1961).
[14] C. Wagner, Z. Elektrochem. **65**, 581 (1961).
[15] H. Furukawa, Adv. Phys. **34**, 703 (1985).
[16] A.J. Bray, Adv. Phys. **43**, 357 (1994).
[17] A.J. Ardell, Acta Metall. **20**, 61 (1972).
[18] A.D. Brailsford and P. Wynblatt, Acta Metall. **27**, 489 (1979).
[19] J.A. Marqusee and J. Ross, J. Chem. Phys. **80**, 536 (1984).
[20] P.W. Voorhees, J. Stat. Phys. **38**, 231 (1985).
[21] M. Marder, Phys. Rev. A **36**, 858 (1987).
[22] J.H. Yao, K.R. Elder, H. Guo, and M. Grant, Phys. Rev. B **47**, 14 110 (1993).
[23] J. Alkemper, V.A. Snyder, N. Akaiwa, and P.W. Voorhees, Phys. Rev. Lett. **82**, 2725 (1999).
[24] P.W. Voorhees and M.E. Glicksman, Acta Metall. **32**, 2001 (1984).
[25] P.W. Voorhees and M.E. Glicksman, Acta Metall. **32**, 2013 (1984).
[26] C.W.J. Beenakker, Phys. Rev. A **33**, 4482 (1986).
[27] N. Akaiwa and P.W. Voorhees, Phys. Rev. E **49**, 3860 (1994).
[28] R.J. White, Mater. Sci. Eng. **40**, 15 (1979).
[29] M. Strobel, S. Reiss, and K.-H. Heinig, Nucl. Instrum. Methods Phys. Res. B **120**, 216 (1996).
[30] M. Strobel, K.-H. Heinig, and W. Möller, Radiat. Eff. Defects Solids **141**, 99 (1997).
[31] A.B. Bortz, M.H. Kalos, J.L. Lebowitz, and M.A. Zendejas, Phys. Rev. B **10**, 535 (1974).
[32] M. Rao, M.H. Kalos, J.L. Lebowitz, and J. Marro, Phys. Rev. B **13**, 4328 (1976).
[33] D.A. Huse, Phys. Rev. B **34**, 7845 (1986).
[34] J.G. Amar, F.E. Sullivan, and R.D. Mountain, Phys. Rev. B **37**, 196 (1988).
[35] J. Marro, A.B. Bortz, M.H. Kalos, and J.L. Lebowitz, Phys. Rev. B **12**, 2000 (1975).
[36] A. Sur, J.L. Lebowitz, J. Marro, and M.H. Kalos, Phys. Rev. B **15**, 3014 (1977).
[37] J. Marro, J.L. Lebowitz, and M.H. Kalos, Phys. Rev. Lett. **43**, 282 (1979).
[38] O. Penrose, J.L. Lebowitz, J. Marro, M.H. Kalos, and S. Sur, J. Stat. Phys. **19**, 243 (1978).
[39] O. Penrose, J. L. Lebowitz, and J. Marro (private communication).
[40] M.E.J. Newman and G.T. Barkema, *Monte Carlo Methods in Statistical Physics* (Oxford University Press, Oxford, 1999).
[41] N. Metropolis, A.W. Rosenbluth, M.N. Rosenbluth, A.H. Teller, and E. Teller, J. Chem. Phys. **21**, 1087 (1953).
[42] K.-H. Heinig (unpublished).
[43] D. Stauffer, J. Phys. A **24**, 909 (1991).
[44] M.F. Sykes, D.S. Gaunt, P.D. Roberts, and J.A. Wyles, J. Phys. A **5**, 640 (1972).
[45] M. Strobel, Ph.D. thesis, Technische Universität Dresden, 1999.
[46] C. Jayaprakash and W.F. Saam, Phys. Rev. B **30**, 3916 (1984).
[47] J. Philibert, *Atom Movements, Diffusion and Mass Transport in Solids* (Les Editions de Physique, Les Ulis, 1991).
[48] H.J. Leamy, G.H. Gilmer, K.A. Jackson, and P. Bennema, Phys. Rev. Lett. **30**, 601 (1973).
[49] K.K. Mon, S. Wansleben, D.P. Landau, and K. Binder, Phys. Rev. B **39**, 7089 (1989).
[50] K.K. Mon, D.P. Landau, and D. Stauffer, Phys. Rev. B **42**, 545 (1990).
[51] S. Mantl, Mater. Sci. Rep. **8**, 1 (1992).
[52] H. Furukawa and K. Binder, Phys. Rev. A **26**, 556 (1982).
[53] M. Strobel, K.-H. Heinig, and W. Möller, Comput. Mater. Sci. **10**, 457 (1998).
[54] M. Palard, Ph.D. thesis, Universite de Paris-Sud, 1997.
[55] K. Binder, Phys. Rev. A **25**, 1699 (1982).
[56] M. Hasenbusch and K. Pinn, Physica A **192**, 342 (1993).
[57] C.W.J. Beenakker and J. Ross, J. Chem. Phys. **84**, 3857 (1986).
[58] T. Imaeda and K. Kawasaki, Physica A **186**, 359 (1992).
[59] S. Reiss, Ph.D. thesis, Technische Universität Dresden, 1996.
[60] A.D. Brailsford, J. Nucl. Mater. **60**, 257 (1976).
[61] K. Binder and D. Stauffer, Phys. Rev. Lett. **33**, 1006 (1974).
[62] K. Binder and D. Stauffer, Adv. Phys. **25**, 343 (1976).
[63] K. Binder, Phys. Rev. B **15**, 4425 (1977).
[64] R. Toral and J. Marro, Phys. Rev. Lett. **54**, 1424 (1985).
[65] In this context, all atoms are counted, which are not connected to the bulk layer. This includes very tiny clusters like dimers, trimers, ...
[66] Neglecting a constant term $J(L_xL_yL_z-2N_V)$, which fixes just the total energy of a lattice containing N_V unoccupied sites.